Fundamental investigation of the drying of solid suspensions

Abdulkadir Osman,[1] Lucas Goehring,[2] Alessandro Patti,[1] Hugh Stitt,[3] Nima Shokri[1,*]

[1]School of Chemical Engineering and Analytical Science, The University of Manchester, Manchester M13 9PL, United Kingdom

[2]School of Science and Technology, Nottingham Trent University, Clifton Lane, Nottingham, NG11 8NS, UK.

[3]Johnson Matthey Technology Centre, Billingham TS23 1LB, UK

ABSTRACT: In this work, a comprehensive series of experiments is conducted to investigate the drying behaviour of micro- and nano-sized particle dispersions. To this end, an acoustic levitator was used to study the drying kinetics of single droplets. The temporal evolution of the actual droplets was recorded using a CMOS camera and the solid grains produced at the end of drying were investigated by SEM imaging. At the end of drying, the grains show different morphologies as a function of the particle size, concentration and initial droplet volume. We combine these experimental data to show the drying behaviour is dependent on all the parameters and that the data all collapses when plotted against Péclet number. This resulted in a novel characteristic diagram which allows one to predict the shape of the dried colloidal droplet based on Pé. Our results extend the fundamental understanding of the mechanisms controlling drying of droplet suspensions.

*Corresponding author

Dr. Nima Shokri

School of Chemical Engineering and Analytical Science

Room C26, The Mill

The University of Manchester

Sackville street, Manchester, M13 9PL, UK

Tel: 0441613063980

Email: nima.shokri@manchester.ac.uk

1. INTRODUCTION

The interests and use of colloidal silica as a precursor in various industrial processes is due to its many advantageous properties including low toxicity, chemical stability and high colloidal stability in various conditions.[1-3] It is used in widely in applications such as post-synthesis surface modification,[4,5] drug carriers,[6,7] catalytic supports,[8,9] antifouling coatings,[10,11] and has factored significantly in nano-particle research and particle formation from the drying of suspensions.[12-14]
Understanding the drying of droplet suspensions is of great importance to a variety of processes such as production of catalyst, ceramic and various pharmaceutical products.[15-17] Many of these products, such as paint pigments and milk powders, are manufactured in a complex industrial process typically through spray drying, whereby spray generation followed by solvent evaporation leads to the assembly of dried grains with different characteristics. To improve the efficiency of spray drying and control the morphology of the resulting final grains, it is crucial to develop understanding of the mechanisms governing the drying of droplets. The need to achieve such a more complete know-how is motivating the scientific community to investigate this process.[18]

The drying kinetics of droplets containing suspended particles might be divided into two stages[19], illustrated schematically in Figure 1. During stage-1 drying, the so-called constant rate period, solvent evaporation from the surface results in a constant shrinkage of its size. The volume change over time during this period resembles that of a pure droplet (i.e. in the absence of suspended particles). Stage-2 drying, the so-called falling rate period, begins at the critical moisture content, X_{cr}, when the solvent from the interior of the droplet can no longer keep the entire surface saturated and a shell is formed as a result of particle deposition at the liquid-air interface. Evaporation continues in this stage through the pores of the shell, until the equilibrium moisture content, X_{eq}, is reached. At this point the resulting particles are typically both dry and rigid.

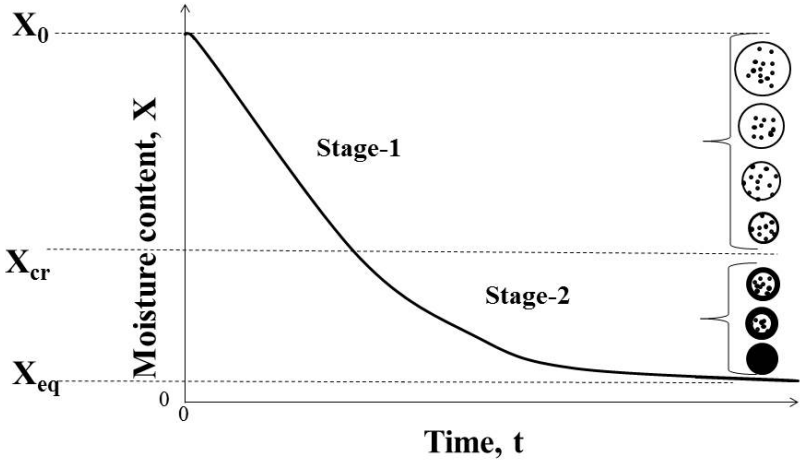

Figure 1. Drying kinetics of droplets containing suspended particles (adopted from[19]).

The morphology and surface properties of dried particles emerging from the drying of suspensions are strongly influenced by the general dynamics of the drying process, the properties of the suspension and the operating conditions.[20-25] Lin and Gentry[20] conducted a comprehensive series of experiments to investigate spray drying drop morphology. They concluded that the dried grain morphology was the result of an interplay between several physico-chemical parameters, such as operating conditions (e.g. temperature), initial particle

concentration, and material properties. Sen et al.[21] investigated the effect of the concentration of suspended particles on the morphological transition in spray drying. In particular, they showed that low particle concentrations led to the creation of a doughnut-like grain as a result of droplet drying. By contrast, due to the reduction of deformation during drying, the same authors showed that increasing particle concentration resulted in the formation of spherical grains. Tsapis et al.[26] illustrated the importance of competition between diffusion and convection during the formation of large porous grains formed as a result of drying of suspensions. Similarly, Trueman et al.[27,28] proposed a model balancing particulate diffusion with the evaporation rate in the drying of films. It was shown that with careful control of the drying dynamics, the presence of different sized particles can be used to manipulate the film morphology resulting in stratification. Baldwin et al.[29] investigated the drying of sessile droplets of aqueous poly (ethylene oxide) (PEO) polymer solutions. Droplets either form a disk-like solid puddle or a tall conical pillar. The final shape of the deposit is shown to depend on many experimentally controllable parameters.

Single droplet drying techniques have been widely used to investigate the drying of solid-liquid droplets as the resulting morphologies have generally been shown to be similar with those produced by industrial spray drying. There are several methods used to investigate the drying of single droplets, some of which involve suspending a droplet from a thin filament[30-34] or free falling of a droplet through a tall tower[35-37]. Early work by Ranz and Marshall[33,34] investigated the rate of evaporation of pure liquid droplets and water drops containing dissolved and suspended solids. Similarly, Sano and Keey[30] monitored the drying of single droplets containing colloidal materials. They proposed a model to describe the formation of internal bubbles during air drying of a droplet containing dissolved solid. They assumed that once the equilibrium vapour pressure of the moisture inside the droplet exceeds the pressure of the ambient air, the grain inflates instantaneously and ruptures into solid hollow spheres playing a significant role in the morphology of final grains.

Using an acoustic levitator to investigate the physics of droplet drying with the associated morphology of the resulting final grain[38-40] offers several advantages compared to other conventional methods; specially, the absence of mechanical contact with the droplet. Kastner et al.[38] experimentally determined the evaporation rates of drops containing water and glass beads by using an acoustic levitator. Both stages of drying were quantified by estimating the droplet volume and measuring the vertical location of the droplet with a CCD camera. Keita et al.[41] recently reported the presence of soft polymer particles suspended in granular packings lead to a significant decrease in the drying rate which was related to the bulk fluid properties.

Despite the recent advances towards a complete understanding of the drying of suspension, there is still a need to contribute to the fundamental aspects of the mechanism that determines the shape of the final grain resulting from the drying of a droplet suspension. Although several groups have investigated the effects of primary particle size on the morphology of the final grains, the complex dynamics of particle deposition and interaction with the evaporating solvent (eventually shaping the morphology of the final particle) are not fully understood yet. Motivated by the relevant impact of the drying of suspensions on key industrial applications, we investigate, from a physical perspective, how a wide range size and concentration of suspended particles influence the drying dynamics and the shape and morphology of the final dried grains. We then combine these experimental data into a dimensionless Péclet number to show that the drying behaviour is dependent on all the parameters and that the data all collapses when plotted against Pé thus resulting in the development of a characteristic diagram relating the shape of the final grain to the dimensionless Péclet number.

2. THEORETICAL CONSIDERATION

During drying, the suspended particles are transported to the interface between air and water via convective transport where the liquid evaporation occurs. This results in preferential particle deposition at the interface. Simultaneously, diffusive transport tends to homogenise the particle concentration over space. This is similar to what occurs drying of granular materials saturated with salty water[42-45] or in solidification of suspensions.[46]

Therefore, the final particle morphology is influenced by the competition between diffusion and convection, which is normally quantified by the dimensionless Péclet number (Pe). The Péclet number for the drying of droplets containing suspended particles can be defined as (Tsapis et al.[26]):

$$\mathrm{Pe} = \frac{R^2}{Dt_{dry}} \tag{1}$$

where R is the radius of droplet, t_{dry} is the drying time and D is the collective diffusion coefficient of the suspended particles. For spherical particles, D can be calculated by using the Stokes-Einstein equation:

$$\mathrm{D} = \frac{k_B T}{6\pi\eta r} \tag{2}$$

where k_B is the Boltzmann's constant, η is the viscosity of the solvent, T the absolute temperature and r the radius of the suspended particles. Note that, for charged particles, such as those used here, D can be enhanced by the inter-particle interactions by about a factor of 10.[47,48]

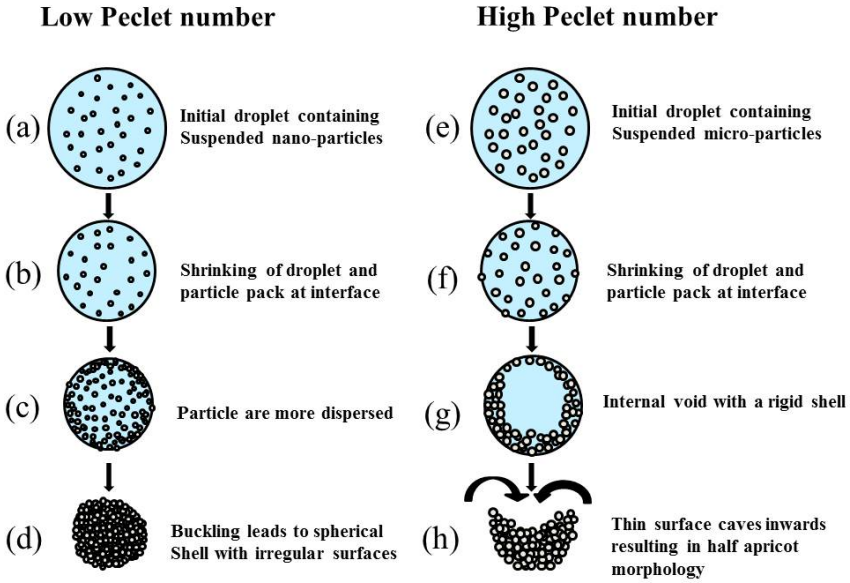

Figure 2. A conceptual picture schematically illustrating the drying of droplets containing nano-sized particles (a)-(d) and micron-sized particles (e)-(h) leading to the final dried grain.

At low Pe, the diffusive transport is comparable to the convective transport (or may be even the dominating transport mechanism at $Pe \ll 1$). Therefore, the particle concentration tends to be uniform through the entire droplet. In such cases, as evaporation proceeds, the droplet

shrinks and a spherical grain forms at the end of the drying process illustrated schematically in Figure 2 (a)-(d). By contrast, when Pe is sufficiently high, convective transport dominates over the diffusive transport. In this case, as evaporation proceeds, this results in a preferential particle accumulation at the evaporation front (i.e. the interface between air and liquid).
As the liquid-vapour interface recedes, packing of solutes leads to the formation of a permeable rigid skin formed at the drop surface. Capillary forces will draw particles together and ultimately van der Waals forces can lock them in place (Tsapis et al.[26]). Particle accumulation at the front leads to thickening of the skin eventually converting the evaporation front to a porous and rigid crust, which encloses the remaining fluid. The subsequent evaporation will continue via flow and evaporation through the crust. Due to the effects of particle settling, the crust formed at the top of the grain is thinner and therefore more susceptible to deformation, compared to the lower region. Such a mechanism may lead to the formation of hollow grains. As the droplet shrinks, the stress generated by the receding vapour-liquid interface may cause breakage in the region where the cohesion of the shell is weaker. The inward collapse at the surface leads to the formation of a half apricot-shape as shown in Figure 2 (e)-(h). Indeed, the crust formation in the drying of suspension droplets can be influenced by the size and concentrations of the suspended particles[49] and the origin of the breakage lies in the inhomogeneity of the shell, which is similar to what has been observed in the drying of latex suspension droplets deposited on a surface.[50]

To validate the above mechanism, we have conducted a comprehensive series of experiments to investigate the effects of Pe on the shape and morphology of grains formed at the end of drying of suspensions. The results of these experiments, which provide the scientific justification to the observations synthesized in Figure 2, are described in the following section.

3. EXPERIMENTAL CONSIDERATION

An ultrasonic acoustic levitator (tec5 AG, UK)) with a standard operating frequency of 58 kHz was used to investigate the drying of suspended droplets and the morphology of the final grains formed at the end of drying. The levitator consists of a reflector, a concave piezoelectric transducer and a micrometer screw to adjust the vertical positioning. A standing wave is generated between the transducer and reflector, in which a single drop can be inserted and suspended in a stationary position. Droplets with diameters in the range of ~0.2-2.5 mm can be levitated below the pressure nodes as a result of axial radiation pressure and radial Bernoulli stress.[51]

All of the droplet experiments were performed using deionised water in ambient conditions. Colloidal silica is used here as the main precursor because of its well-known and established chemistry and its relevance in industrial applciations.[13] To cover a wide range of values, we investigated spherically charge-stabilised dispersions (described and characterised elsewhere) of colloidal silica Ludox HS (Grace, ~220 m^2/g) with radius of 8 nm,[52] Levasil (Azko-Nobel, ~30 m^2/g) 46 nm,[53] latex (~20 m^2/g) 142 nm,[54] and micro-suspensions containing particles with a radius of 0.5 μm (~3 m^2/g), 2.5 μm (0.5 m^2/g) and 5 μm (~0.2 m^2/g, Sigma-Aldrich), respectively. The drying of droplets with particle concentrations of 1, 2, 3, 5, 10, 20 and 30 wt% were investigated with varying droplet volumes of 0.8, 1.1, 1.4, 1.7, 2, 2.3 μL. The drops were inserted into the standing wave using a 5 μL syringe. The chamber is ventilated with a flow rate of 0.5 l/min of air during the course of the evaporation to ensure constant drying conditions.[55] An automatic imaging system was set up to record every minute the temporal evolution of the droplet during drying using a CMOS camera (Canon EOS 700D). The resulting images were manually processed using ImageJ software. The aspect ratio, being

the ratio between horizontal and vertical diameter, and the change in equivalent droplet diameter were calculated during drying. In particular, the cross-sectional area of the droplet, A, was computed from the images and the equivalent diameter, d, was calculated using $d = \sqrt{\frac{4A}{\pi}}$. Each experiment was repeated five times to ensure reproducibility of the data and improve statistics. The resulting dried grains were collected and subjected to SEM imaging (Quanta 200) which enabled us to investigate the morphology and surface characteristics of the final grains as a function of the size and concentration of suspended particles.

4. RESULTS AND DISCUSSION

4.1. Single droplet drying behaviour. A series of images illustrating qualitatively how the droplets evolve as drying proceeds is shown in Figure 3. The drying behaviour of silica-water suspensions initially resembles that of a pure droplet, i.e. a constant decrease in the volume as the bulk of the liquid is evaporated. At the end of drying of micro and nano-suspensions, a solid grain is formed.

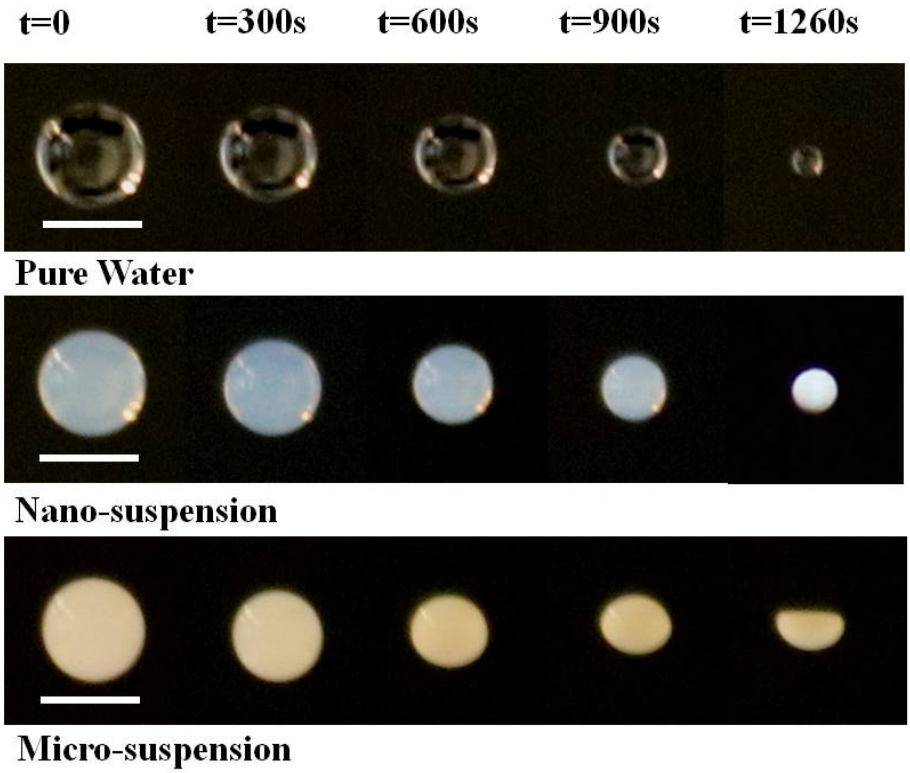

Figure 3. Typical images captured at different times illustrate the evolution of pure water droplets and drops containing 1% suspended micron-sized particles (r~ 2.5 μm) and nano-sized particle (Levasil, r~ 46 nm). In all cases the initial droplet volume was 2.3 μl. The time at top indicates the elapsed time from the onset of each experiment and the scale bar represents 1.6 mm.

Using the recorded images, we could quantify the temporal evolution of each drop (Figure 4). Contrary to the case of drying of pure water droplets, solvent evaporation from suspensions leads to shell formation. In such situations, droplet shrinking ceases at a certain diameter corresponding to the size, of the dried grain. The results obtained shows how the evaporation rates from the droplet suspension are modified as particle concentration changes. Note that

each experiment was conducted 5 times, but since the standard deviation between experiments was small and the data was robustly reproducible, to improve the clarity the error bars were not added to Figure 4. The drying behaviour of droplets containing lower particle concentrations is quite close to that of a pure water droplet. However, as the concentration of suspended particles increases, the duration of stage-1 drying decreases. This is attributed to the presence of less water in the droplet leading to an earlier formation of the final grains.

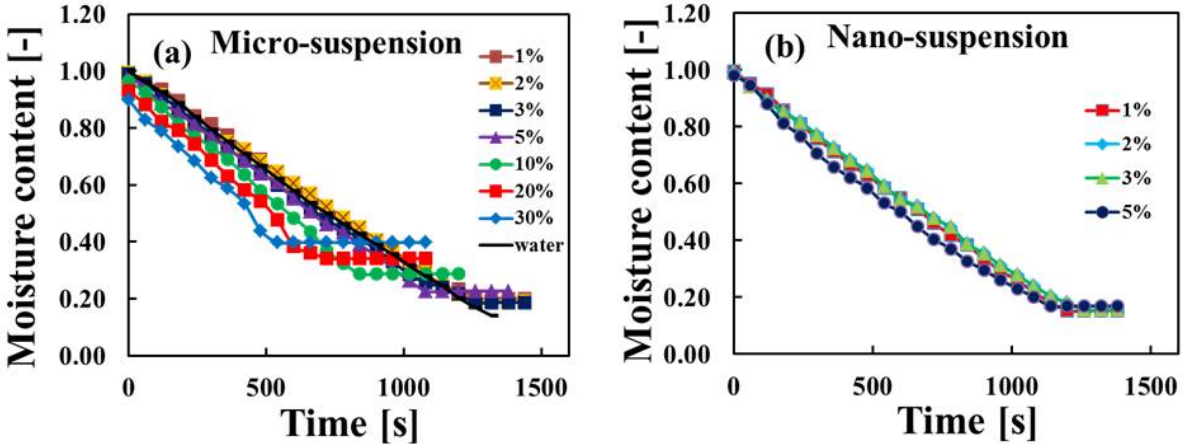

Figure 4. The effect of particle concentration on the drying dynamics of droplet containing micron-sized particles of r~2.5 µm (a) and Ludox nano-sized particles of r~8 nm (b) at an initial droplet volume of 2.3 µl. The legend indicates the initial particle concentration.

The evaporation rate (i.e. the slope of the line in Figure 4) was relatively constant in the case of nano-sized particle dispersion probably because of the narrow ranges of the concentrations. However, in the case of micro-suspension droplets, as particle concentration increased, slightly higher evaporation rates during stage-1 were observed. These results seem to be consistent with other research which found the presence of particles enhanced the evaporation of small droplets.[56,57] This is explained due to particles near the interface such that part of the particles along the air-water interface, covered by liquid, are exposed into the ambient air and the remaining part is partially submerged in the liquid. This enhances the evaporation rate (possibly due to the enhanced vaporization surface) as has been shown in Zhang et al.[56] It is therefore to be expected that droplets containing higher particle concentration at the interface would have a slightly higher evaporation rate as seen in Figure 4.

In addition to the equivalent droplet diameter, the evolution of the aspect ratio (AR) over time in the case of droplets containing micro and nano-sized dispersions was measured as presented in Figure 5. We observed significant deviation from sphericity towards the end of the drying of droplets containing micro-particles (Figure 5 (b)). Such an increase in AR was not observed in the case of nano-suspension. SEM analysis of the obtained grains shows that a half apricot-like morphology is typically formed from the drying of micro-suspensions. This is shown in Figure 6 (a) and (b). However, in the case of nano-suspensions, the droplets maintain their shape and shrink isotropically during the evaporation process forming an agglomerated spherical grain as presented in Figure 6 (c). During drying, instabilities can arise as a result of capillary forces which are applied through a relatively thin layer in the shell. Such deformation occurs as soon as the outer shell is capable of responding as an elastic solid (i.e. high enough yield stress) and can lead to instabilities that causes

buckling.[58,59] As buckling involves a mix of compressional and extensional regions, it is often associated with additional fracturing, as observed in Figure 6 (d), as rigidity is also the prerequisite for fracture. Thus, it is clear from the captured images of the final dried grains coupled with SEM analysis that the morphology and surface characteristics are significantly influenced by the size and concentration of the suspended particles. The governing mechanism is further explained in the following section.

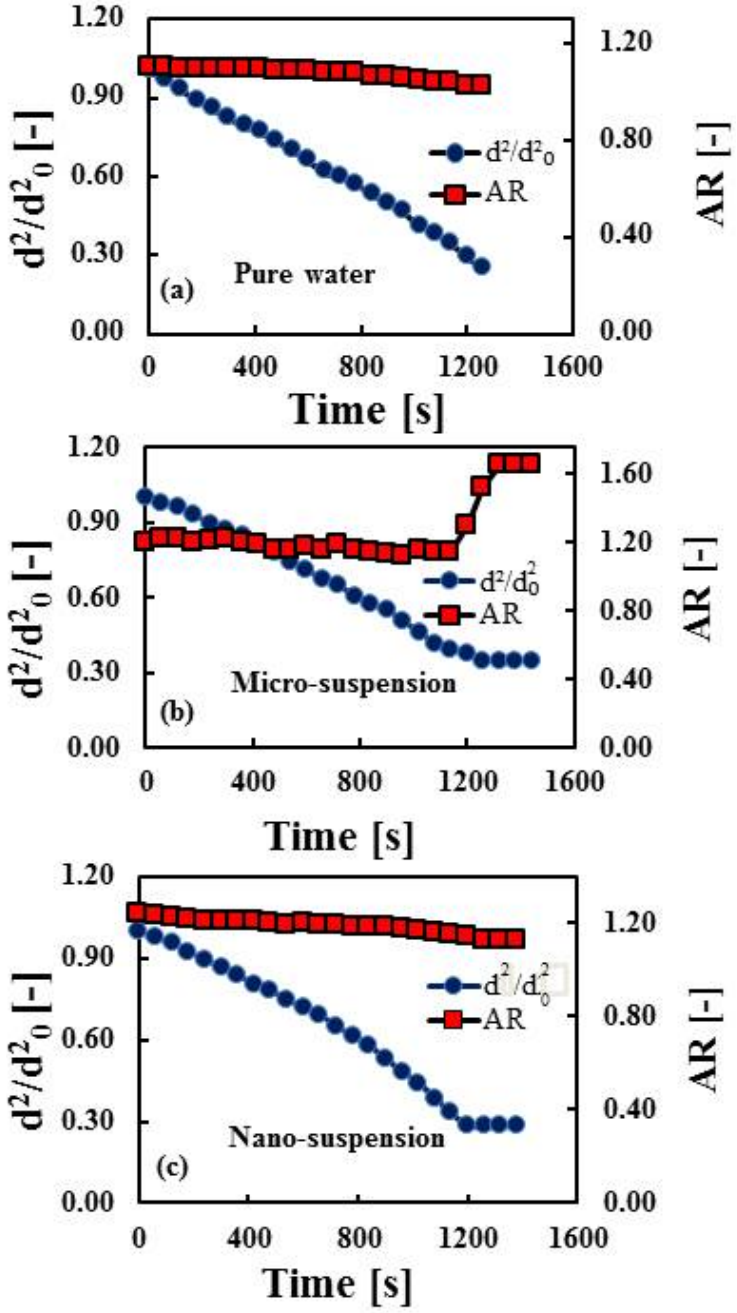

Figure 5. The measured equivalent diameter, *d*, and aspect ratio (*AR*) of a) pure water b) 1% micro-suspension (radius of 2.5 µm) and c) 1% nano-suspension (radius of 8 nm) droplets with an initial droplet volume of 2.3 µl. d_0 corresponds to the initial droplet diameter.

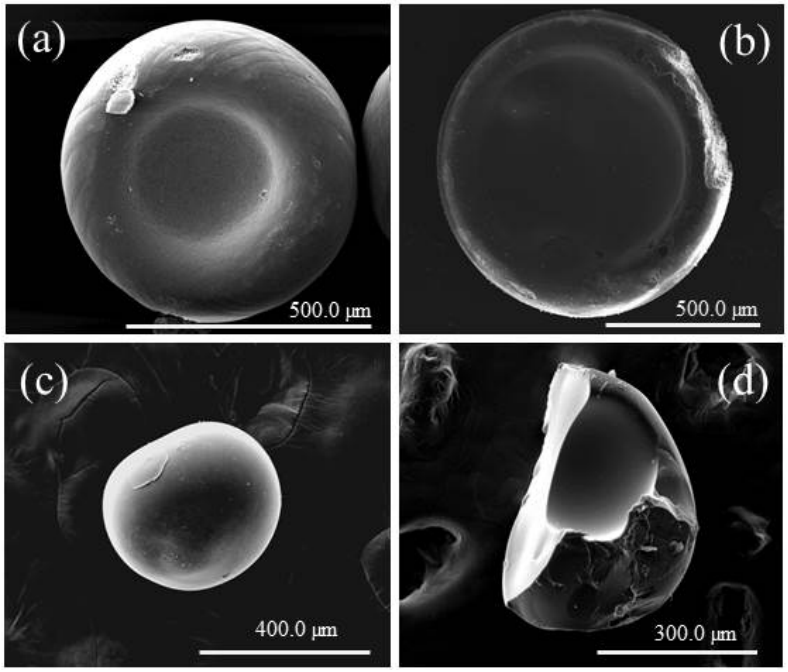

Figure 6. SEM images of the final grains obtained from the drying of droplets containing (a) 1% and (b) 30% concentration of micro-particles (*r*~ 2.5 μm) and (c) 1% and (d) 30% concentration of Ludox nano-particles (*r*~ 8 nm). In all cases the initial droplet volume was 2.3 μl.

4.2. Influence of particle size on grain properties. We have estimated the Péclet number for drying of micro and nano-sized dispersions in our experiments using eq (1-2). For *T*= ~*23*˚C, *r*~ *2.5* μm and $\eta = 9.33\times10^{-4}$ Pa s (assuming viscosity of pure water at *T*~*23*˚C), the Stokes-Einstein diffusivity for micro-silica particles is estimated as 9.3×10^{-14} m^2/s which results in Pe ≅5000 for a drying time of ~ 1200 s. The large Pe value indicates preferential particle accumulation at the interface between liquid and air, making it more susceptible to deformation which is indeed in agreement with the SEM images of the grains formed at the end of drying of micro-suspensions presented in Figure 6 (a) and (b). The formation of hollow grains from droplet drying is generally the result of formation of an internal void during the first drying period which depends on the ability of the particles to diffuse inside the droplet.[60,61] In this case, the diffusivity of the particles is dependent on the particles size: micro-particles have a much lower diffusion coefficient than nano-particles and therefore cannot diffuse easily to centre of the droplet as illustrated in Figure 2 (e)-(h). In addition to the hollow shape, the presence of shear bands can also be seen on the surfaces of the dried grains (Figure 6 (a)).[62]

In the case of nano-suspensions, with particles of radius 8 nm, the diffusion coefficient is estimated as 3.33×10^{-11} m^2/s with the corresponding *Pe*≅14. Therefore, in the case of drying of nano-suspension, the relatively small Pe value indicates that the diffusive transport is comparable with the convective transport. This should result in homogeneous particle distribution and deposition during drying which eventually leads to an agglomerated dense spherical grain, (Figure 2 (a)-(d)), which is in agreement with the SEM images of the grain formed at the end of drying of nano-suspension at low concentrations presented in Figure 6 (c).

However, during drying of nano-suspension droplets containing high particle concentration, buckling and fragmentation of the grains may occur (Figure 6 (d)). In such cases, the

buckling of a colloidal droplet can be reduced by forming a suspension of aggregates by increasing the ionic strength such that it leads to a reduction in the magnitude and range of the repulsive electrostatic energy thus inducing aggregation between particles.[63] Drying experiments were performed with nano-particles (30%) in a NaCl salt solution (0.2 M) which resulted in solid grains with cracks on the surfaces clearly visible as shown in Figure 7. The reduction buckling of the grains is due to an increase in the permeability of the shell to solvent which is in agreement with the those of previous studies by Lintingre et al.[64]

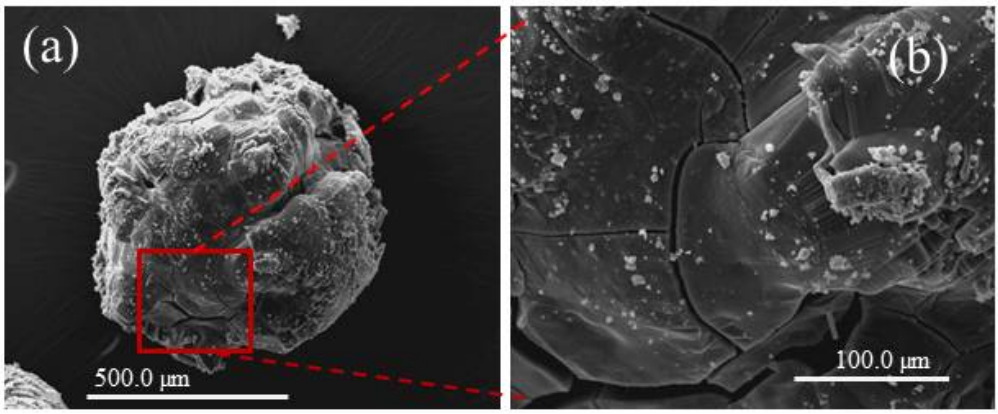

Figure 7. SEM images of (a) final grains obtained from the drying of nano-suspension (r~ 8 nm) droplets in 0.2 M NaCl solution and (b) shows crack formation on the surface of the grains.

4.3. Péclet number and morphology. The experimental parameters of particle size, droplet volume, and particle concentrations were all observed to influence the final grain shape. Here we systematically alter each parameter and record the drying dynamics. Figure 8 show the final grain obtained from the drying of droplets with varying (a) particle size (V_0 =1.4 μl) and (b) initial droplet volume (r = 0.5 μm) plotted against the observed aspect ratio. From this, we can see a clear morphological transformation from spherical to half apricot dried grains. Small particles, i.e. low Pe, leads to spherical grains as diffusive transport dominate convection[65,66] thus the particles tends to homogenise over space and the droplets shrink isotropically to form uniform spherical grain illustrated in Figure 8 (a). Larger particles lead to the formation of hollow grains which is driven by inhomogeneity of the shell. Similarly, at larger droplets, i.e. higher Pe, hollow grains are formed and smaller droplets tend to form grains that remain intact i.e. not hollow. The transition stage i.e. between spherical and half apricot morphology occurs in the intermediate Pe range in which the obtained solid grains have an AR of ~1.3 similar to an elongated grain in shape (as seen in Figure 8 (b) in the lower range of Pe).

Predicting the morphology of the final grains formed as a result of drying of suspension based on the value of Péclet number will be useful to provide an effective representation of the primary forces determining the shape of the final grains. Similarly to the classification of flow regimes based on the Reynolds number in fluid mechanics, the patterns formation in frictional fluid dynamics,[67] or the classification of displacement patterns during multiphase flow in porous media,[68] such a characteristic diagram will be a guideline to associate specific shapes of final grains to a given range of Péclet numbers. To obtain such a characteristic diagram, we combine these experimental data into a dimensionless Péclet number to show that the drying behaviour is dependent on all the parameters (i.e. r, V_0 and X_0) and that the data all collapses when plotted against Pe.

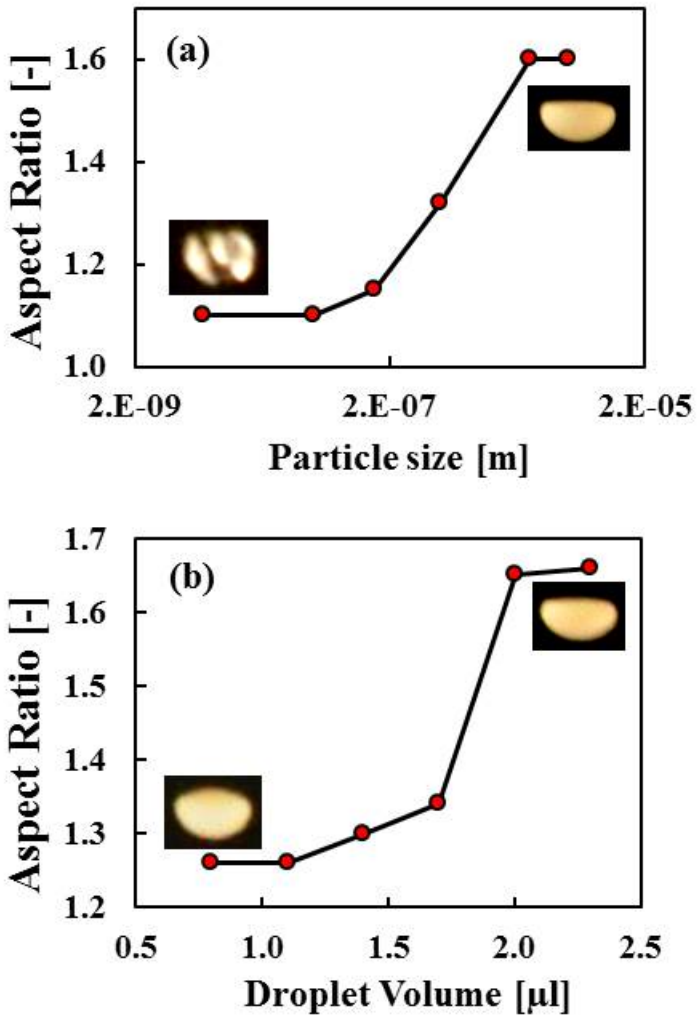

Figure 8. Aspect ratio of the dried grains are plotted against (a) Particle size (V_0 =1.4 µl) (b) Droplet volume (PS= 0.5 µm).

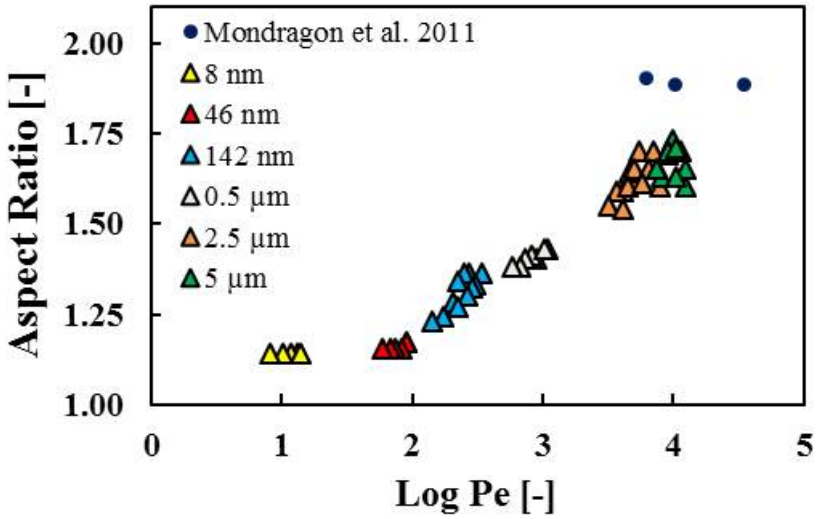

Figure 9. Characteristic diagram showing the aspect ratio (AR) vs Peclet number (Pe) obtained from the drying of suspensions of different particle sizes (*r*), initial volumes (V_0) and initial particle concentrations (X_0).

The phase diagram illustrating the relationship between the particle aspect ratio and the Pe is presented in Figure 9. It shows one can accurately predict the shape of the dried colloidal droplet based on Pé. Note that the closer the *AR* to one, the closer is the shape of final particle to a perfect sphere. The points plotted in Figure 9 include experimental results adopted from Mondragon et al.[39] where the Pe was estimated for initial droplet volumes of 0.7 and 0.07 µL. In their experiments, the 0.07 µL droplets contains two different concentrations, which results in two Pe numbers, because of the effects of particle concentration on the drying rate and consequently drying time (using eq (1-2)). For *T*= 363.15 K, *r*~ *6.5* µm and $\eta = 3.15\times10^{-4}$ Pa·s (assuming viscosity of pure water at 363.15 K), the diffusion coefficient is estimated as 1.3×10^{-13} m^2/s which results in Pe = ~36000 and 6400 for the drying time of ~ 75 and 65 s, respectively. The morphology of the final dried grains obtained deviates significantly from sphericity as seen in the measured aspect ratio (see Figure 3(a) and (b) from Mondragon et al.[39]). Thus, we show that our characteristics diagram can be used to accurately predict the final grains obtained from the drying of droplet suspensions. For example, here we would expect smaller particle size with low Pé to form grains in the transition stage i.e. elongated but not hollow grains (similar to that observed in Figure 8 (b)). A further decrease in these parameters would lead to the formation of spherical grains.

5. SUMMARY AND CONCLUSION

The drying of a suspension and the associated grain morphology formed as a result of drying is a function of a number of parameters including, but not limited to, particle size, particle concentration, and droplet volume. The aim of the present work was to investigate the drying kinetics of droplet suspensions and the resulting morphology of grains at the end of drying, which is important to a variety of industrial applications. Single droplet drying experiments were performed using an acoustic levitator and a CMOS camera to record the temporal evolution of the drying droplets as a function of suspended particle size and concentration. SEM was used to observe the characteristics of the final dried grain obtained at the end of each experiment. We show that the drying behaviour and the assembly of the final grains are significantly influenced by the particle size, particle concentration and initial droplet volume. The observed morphological difference was shown to be the result of the competition between diffusion and convection during drying. We combine these experimental data into a dimensionless Péclet number to show that the drying behaviour is dependent on all the parameters. This resulted in a novel characteristic diagram which allows one to accurately predict the shape of the dried colloidal droplet based on Pé.

ACKNOWLEDGEMENTS

We would like to acknowledge the UK Engineering and Physical Sciences Research Council (EPSRC) to provide the PhD studentship for Abdulkadir Osman and Johnson Matthey for additional funding of this project.

REFERENCES

(1) Liberman, A.; Mendez, N.; Trogler, W. C.; Kummel, A. C. Synthesis and Surface Functionalization of Silica Nanoparticles for Nanomedicine. *Surf. Sci. Rep*. **2014**, *69*, 132−158.
(2) Wang, J.; Shah, Z. H.; Zhang, S.; Lu, R. Silica-Based Nanocomposites via Reverse Microemulsions: Classifications, Preparation and Applications. *Nanoscale* **2014**, *6*, 4418−4437.
(3) Guerrero-Martínez, A.; Perez-Juste, J.; Liz-Marzan, L. M. Recent Progress on Silica Coating of Nanoparticles and Related Nanomaterials. *Adv. Mater*. **2010**, *22*, 1182−1195.
(4) Mugica, L. C.; Rodríguez-Molina, B.; Ramos, S.; Kozina, A. Surface Functionalization of Silica Particles for Their Efficient Fluorescent and Stereo Selective Modification. *Colloids Surf. A* **2016**, *500*, 79−87.

(5) Qiao, B.; Liang, Y.; Wang, T.-J.; Jiang, Y. Surface Modification to Produce Hydrophobic Nano-Silica Particles Using Sodium Dodecyl Sulfate as a Modifier. *Appl. Surf. Sci*. **2016**, *364*, 103−109.
(6) Geszke-Moritz, M.; Moritz, M. APTES-Modified Mesoporous Silicas as the Carriers for Poorly Water-Soluble Drug. Modeling of Diflunisal Adsorption and Release. *Appl. Surf. Sci*. **2016**, *368*, 348−359.
(7) Rajanna, S. K.; Kumar, D.; Vinjamur, M.; Mukhopadhyay, M. Silica Aerogel Microparticles from Rice Husk Ash for Drug Delivery. *Ind. Eng. Chem. Res*. **2015**, *54*, 949−956.
(8) Xie, W.; Hu, L.; Yang, X. Basic Ionic Liquid Supported onMesoporous SBA-15 Silica as an Efficient Heterogeneous Catalyst for Biodiesel Production. *Ind. Eng. Chem. Res*. **2015**, *54*, 1505−1512.
(9) Nasir Baig, R. B.; Varma, R. S. Magnetic Silica-Supported Palladium Catalyst: Synthesis of Allyl Aryl Ether in Water. *Ind. Eng. Chem. Res*. **2014**, *53*, 18625−18629.
(10) Zhu, L. J.; Zhu, L. P.; Jiang, J. H.; Yi, Z.; Zhao, Y. F.; Zhu, B. K.; Zhu, L. J.; Zhu, L. P.; Jiang, J. H.; Yi, Z.; Zhao, Y. F.; Zhu, B. K.; filtration Membranes with Poly(2-hydroxyethyl methacrylate) Grafted Silica Nanoparticles as Additive. *J. Membr. Sci*. **2014**, *451*, 157−168.
(11) Huang, J.; Zhang, K.; Wang, K.; Xie, Z.; Ladewig, B.; Wang, H. Fabrication of Polyethersulfone-Mesoporous Silica Nanocomposite Ultrafiltration Membranes with Antifouling Properties. *J. Membr. Sci*. **2012**, *423−424*, 362−370.
(13) Bergna, H. E.; Roberts, W. O. *Colloidal Silica Fundamentals and Applications*; CRC Press: Boca Raton, pp 575−588, 2006.
(14) Cho, Y-S. Fabrication of Hollow or Macroporous Silica Particles by Spray Drying of Colloidal Dispersion. *J. Disp. Sci. Tech.*, **2016**, *37*, 23-33.
(15) Masters, K. *Spray Drying Handbook*; Longman Scientific & Technical: Harlow, England, 5th edn, 1991.
(16) Vervaet, C.; Remon, J. P. Continuous granulation in the pharmaceutical industry. *Chem. Eng. Sci*. **2005**, *60*, 3949–3957.
(17) Rahaman, M. N. *Ceramic Processing and Sintering*; Marcel Dekker Inc: New York, 1995.
(18) Lintingre, E.; Lequeux, F.; Talini, L.; Tsapis, N. Control of particle morphology in the spray drying of colloidal suspensions. *Soft Matter* **2016**, *11*, 7435-7444.
(19) Mezhericher, M.; Levy, A.; Borde, I. Theoretical models of single droplet drying kinetics: A review. *Drying Technol*. **2010**, *28*, 278-293.
(20) Lin, J. C.; Gentry, J. W. Spray drying drop morphology: Experimental study. *Aerosol Sci. Technol.* **2003**, *37*, 15–32.
(21) Sen, D.; Mazumder, S.; Melo. J. S.; Khan, K.; Bhattyacharya, S.; D'Souza, S. F. Evaporation driven self-assembly of a colloidal dispersion during spray drying: Volume fraction dependent morphological transition. *Langmuir* **2009**, *25*, 6690–6695.
(22) Cheow, W. S.; Li, S.; Hadinoto, K.; Spray drying formulation of hollow spherical aggregates of silica nanoparticles by experimental design. *Chem. Eng. Res. Des*. **2010**, *88*, 673–685.
(23) Elversson, J.; Millqvist-fureby, A.; Alderborn, G.; Elofsson, U. Droplet and particle size relationship and shell thickness of inhalable lactose particles during spray drying. *J. Pharm. Sci*. **2003**, *92*, 900-910.
(24) Vehring, R.; Pharmaceutical particle engineering via spray drying. *Pharm. Res*. **2008**, *25*, 999-1022.
(25) Iskandar, F.; Gradon, L.; Okuyama, K. Control of the morphology of nanostructured particles prepared by the spray drying of a nanoparticle sol. *J. Colloid Interface Sci*. **2003**, *265*, 296–303.
(26) Tsapis, N.; Bennett, D.; Jackson, B.; Weitz, D. A.; Edwards, D. A. Trojan particles: Large porous carries of nanoparticles for drug delivery. *Proc Natl. Acad. Sci. U.S.A*. **2002**, *99*, 12001–12005.
(27) Trueman, R. E.; Lago Domingues, E,; Emmett, S N.; Murray, M.; Routh, A F.; Auto-stratification in drying colloidal dispersions: a diffusive model *J. Colloid Interface Sci.* **2012**, *377*, 207–12.
(28) Trueman, R. E.; Lago Domingues, E.; Emmett, S. N.; Murray, M.; Keddie, J. L.; Routh, A. F. Autostratification in drying colloidal dispersion: Experimental investigation. *Langmuir* **2012**, *18*, 3420–8.
(29) Baldwin, K. A.; Granjard, M.; Willmer, D I.; Sefiane, K.; Fairhurst, D. J. Drying and deposition of poly(ethylene oxide) droplets determined by Peclet number. *Soft Matter* **2011**, *12*, 3998–4004.

(30) Sano, Y.; Keey, R. B. The drying of a spherical-particle containing colloidal material into a hollow sphere. *Chem. Eng. Sci*. **1982**, *37*, 881–889.
(31) Charlesworth, D. H.; Marshall, W. R. J. Evaporation from drops containing dissolved solids. *AIChE J*. **1960**, *6*, 9–23.
(32) Walton, D. E.; Mumford C. J. The morphology of spray-dried particles. *Trans. Inst. Chem. Eng*. **1999**, *77*, 442–460.
(33) Ranz, W. E.; Marshall, W. R. J.; Evaporation of drops part 1. *Chem. Eng. Prog*. **1952**, *48*, 141–146.
(34) Ranz, W. E.; Marshall, W. R. J.; Evaporation of drops part 2. *Chem. Eng. Prog*. **1952**, *48*, 173–180.
(35) El-Sayed, T. M.; Wallack, D. A.; King, C. J. Changes in particle morphology during drying of drops of carbohydrate solutions and food liquids - part 1: Effects of composition and drying conditions. *Ind. Eng. Chem. Res*. **1990**, *29*, 2346–2354.
(36) Wallack, D. A.; El-Sayed, T. M.; King, C. J. Changes in particle morphology during drying of drops of carbohydrate solutions and food liquids - part 2: Effects on drying rate. *Ind. Eng. Chem. Res*. **1990**, *29*, 2354–2357.
(37) Vehring, R. Foss, W. R. ; Lechuga-Ballesteros, D. Particle formation in spray drying *Aerosol Sci*. **2007**, *38*, 728–746.
(38) Kastner, O.; Brenn, G.; Rensink, D.; Tropea, C. The Acoustic Tube Levitator – A Novel Device for Determining the Drying Kinetics of Single Droplets. *Chem. Eng. Technol*. **2001**, *24*, 335–339.
(39) R. Mondragon, L. Hernandez, J. E. Julia, J. C. Jarque, S. Chiva, B. Zaitone, and C. Tropea, *Chem. Eng. Sci*. **2011**, *66*, 2734–2744.
(40) Yarin, A. L.; Brenn G.; Kastner, O.; Tropea, C. Drying of acoustically levitated droplets of liquid-solid suspensions: Evaporation and crust formation. *Phys. Fluids* **2002**, *14*, 2289–2298.
(41) Keita E.; Kodger; T. E.; Faure, P.; Rodts, S.; Weitz, D. A.; Coussot, P. Water retention against drying with soft-particle suspensions in porous media. *Phys. Rev. E*. **2016**, *94*, 033104.
(42) Guglielmini, L. Gontcharov, A. Aldykiewicz Jr, A. J. Stone, H. A. Drying of salt solutions in porous materials: Intermediate-time dynamics and efflorescence *Phys. Fluids* **2008**, *20*, 077101.
(43) Shokri, N.; Pore-scale dynamics of salt transport and distribution in drying porous media *Phys. Fluids*, **2014,** *26*, 012106.
(44) Norouzi Rad, M.; Shokri, N.; Keshmiri, A.; Withers, P. J. Effects of grain and pore size on salt precipitation during evaporation from porous media: A pore-scale investigation. *Transp. Porous Med*. **2015,** *110*, 281–294.
(45) Shokri-Kuehni, S. M. S.; Vetter, T.; Webb, C.; Shokri, N. New insights into saline water evaporation from porous media: Complex interaction between evaporation rates, precipitation, and surface temperature. *Geophys. Res. Lett*. **2017**, *44*, 5504–5510, doi:10.1002/2017GL073337.
(46) Peppin, SSL.; Elliott, JAW.; Worster, MG. Solidification of colloidal suspensions. *J. Fluid Mech*., **2006**, *554*, 147–166.
(47) Goehring, L.; Li, J.; Kiatkirakajorn, P-C. Drying paint: from micro-scale dynamics to mechanical instabilities. *Phil. Trans. R. Soc. A*. **2017**, *375*, 20160161.
(48) Loussert, C.; Bouchaudy, A.; Salmon, J.B. Drying dynamics of a charged colloidal dispersion in a confined drop. *Phys. Rev. Fluids*, **2016**, *1*, 084201.
(49) Leng, J. Drying of a colloidal suspension in confined geometry. *Phys. Rev. E*. **2010,** *82*, 021405.
(50) Pauchard, L; Couder, Y. Invagination during the collapse of an inhomogeneous spheroidal shell. *Europhys. Lett*. **2004**, *66*, 667–673.
(51) Vandaele, V.; Lambert, P.; Delchambre, A. Non-contact handling in microassembly: Acoustical levitation. *Precis. Eng*. **2005**, *29*, 491–505.
(52) Goertz, V.; Dingenouts, N.; Nirschl, H. Comparison of Nanometric Particle Size Distributions as Determined by SAXS, TEM and Analytical Ultracentrifuge *Part. Part. Syst. Char*. **2009**, *26*, 17−24.
(53) Boulogne, F.; Pauchard, L.; Giorgiutti-Dauphine, F.; Botet, R.; Schweins, R.; Sztucki M.; Li J.; Cabane, B.; Goehring, L. Structural anisotropy of directionally dried colloids. **2014**, *105*, 38005.
(54) Yow, H N.; Goikeotxea, M.; Goehring, L.; Routh, A F. Effect of film thickness and particle size on cracking stress in drying latex films *J. colloid Interface Sci*, **2010**, *352*, 542-548.
(55) Yarin, A. L.; Brenn, G.; Kastner, O.; Rensink, D.; Tropea, C. Evaporation of acoustically levitated droplets. *J. Fluid Mech*., **1999**, *399*, 151-204.

(56) Zhang, W.; Shen, R.; Lu, K.; Ji, A.; Cao, Z. Nanoparticle enhanced evaporation of liquids: A case study of silicone oil and water *AIP Adv*. **2012**, *2*, 042119.
(57) Hughes, R. B.; Stampfer Jr, J. F. Enhanced Evaporation of Small, Freely Falling Water Drops Due to Surface Contamination. *J. Atm. Sci*. **1971**, *28*, 1244.
(58) Hutchinson. JW. Buckling of spherical shells revisited. *Proc. R. Soc. A* **2016** *472* 20160577.
(59) Tsapis, N.; Dufresne, E. R.; Sinha, S. S.; Riera, C. S.; Hutchinson, J. W.; Mahadevan, L.; Weitz, D. A. Onset of Buckling in Drying Droplets of Colloidal Suspensions. *Phys. Rev. Lett*. **2005**, *94*, 018302.
(60) Walker, W. J.; Reed, J. S.; Verma S. K.; Influence of Slurry Parameters on the Characteristics of Spray-Dried Granules. *J. Am. Ceram*. Soc. **1999**, *82*, 1711–1719.
(61) Bertrand, G.; Filiatare, C.; Mahdjoub, H.; Foissy, A.; Coddet, C. Influence of slurry characteristics on the morphology of spray-dried alumina powders. *J. Eur. Ceram. Soc*. **2003**, *23*, 263–271.
(62) Kiatkirakajorn, P.-C.; Goehring, L. Formation of Shear Bands in Drying Colloidal Dispersions *Phys. Rev. Lett.* **2015**, *115*, 088302.
(63) Luckham, P. F.; Rossi, S. The colloidal and rheological properties of bentonite suspensions. *Adv. Colloid Interface Sci*. **1999**, *82*, 43–92.
(64) Lintingre E.; Ducouret, G.; Lequeux, F.; Olanier L.; Perie, T.; Talini, L. Controlling the buckling instability of drying droplets of suspensions through colloidal interactions. *Soft Matter* **2015**, *11*, 3660–3665.
(65) N, Shokri.; Zhou, P.; Keshmiri A. Patterns of Desiccation Cracks in Saline Bentonite Layers. *Trans. Porous. Med*. **2015**, *110*, 333-344.
(66) N, Shokri.; Lehmann, P.; Vontobel, P.; Or, D. Drying front and water content dynamics during evaporation from sand delineated by neutron radiography. *Water Resour. Res*. **2008**, *44*, W06418.
(67) Sandnes, B.; Flekkøy, E. G.; Knudsen, H. A.; Måløy, K. J.; See, H. Patterns and flow in frictional fluid dynamics. *Nat. Commun*. **2011**, *2*, 288.
(68) Or, D. Scaling of capillary, gravity and viscous forces affecting flow morphology in unsaturated porous media. *Adv. Water Resour*. **2008**, *31*, 1129–1136.